International Journal of Heat and Mass Transfer 77 (2014) 1115–1123

Contents lists available at ScienceDirect

International Journal of Heat and Mass Transfer

journal homepage: www.elsevier.com/locate/ijhmt

Performance and two-phase flow pattern for micro flat heat pipes

Kai-Shing Yang [a], Chen-Chuan Lin [b], Jin-Cherng Shyu [b], Chih-Yung Tseng [a], Chi-Chuan Wang [c,*]

[a] Green Energy and Environment Research Lab., Industrial Technology Research Institute, Hsinchu 31040, Taiwan
[b] Department of Mechanical Engineering, National Kaohsiung University of Applied Sciences, Kaohsiung 80778, Taiwan
[c] Department of Mechanical Engineering, National Chiao Tung University, Hsinchu 30010, Taiwan

ARTICLE INFO

Article history:
Received 1 April 2014
Received in revised form 18 June 2014
Accepted 19 June 2014
Available online 9 July 2014

Keywords:
Heat pipe
Vapor chamber
Two-phase flow
Thermal resistance

ABSTRACT

In this study, thermal performance and flow visualization of a double layer flat micro vapor chamber are reported. Two micro vapor chambers having pin fin and pin fin array support structure are fabricated and tested. The micro vapor chambers are composed of silicon and glass wafers having an overall size of $35 \times 40 \times 1.525$ mm. Test results show that both the pin fin and pin fin array vapor chambers show an appreciably lower thermal resistance as compared to the solid silicon counterpart, the thermal resistance of the pin fin vapor chamber is about 52–60% of the solid silicon whereas the corresponding thermal resistance of pin fin array is only 17–20% of the solid silicon. The thermal resistance of the pin fin vapor chamber is moderately increased subject to the increase of supplied power whereas opposite trend is encountered for the pin fin array. The phenomenon is associated with the influence of dry-out phenomenon. It is found that the pin fin array vapor chamber is still in function even for an upside-down arrangement. The thermal resistance, however, is reduced with the rise of tilt angle, and the vertical arrangement gives the lowest thermal resistance. However, the thermal resistance is considerably increased if the heat source is placed upwards, and the corresponding thermal resistance for an upside-down heat source can be threefold higher than that of the vertical arrangement.

1. Introduction

In recent year, solid state lighting (e.g. LEDs) had significantly penetrated into and replaced conventional lighting market. This is associated with some of its distinguished features such as longevity, high efficiency, and environmental benign. Despite the rapid growth of LED lighting, the margin profit is also falling especially for the low power LEDs. Hence, high power LED applicable for some high-end applications had attracted a lot attention for the developers and manufacturers. Normally the high power LEDs require massive heat sink for heat dissipation, this apparently impairs the willingness of the purchase of such products from the viewpoint of the consumers for they normally expect a small volume and a low weight of the LED lighting. Currently, some manufactures had unveiled 50 W LED chip packaged in an area less than 1 cm^2 [1]. The design is capable of delivering 4300 lm brightness but also accompanied with a huge heat flux of 61.73 W/cm^2. With this enormous heat flux, a local hot spot may develop and damages the LED accordingly [2]. As a consequence, thermal management of the high power LED becomes a drastic issue that must be resolved during the design phase.

Normally, metal or ceramics are considered as the substrate of the conventional high power LED packaging. The comparatively low thermal conductivity of the substrates may jeopardize the heat dissipation path and this becomes even more pronounced when the power is raised further. Hence vapor chamber (flat heat pipe) is regarded as an effective means for high power concentrated heat sources, e.g. LED. The vapor chamber is one of the promising heat transfer devices capable of removing high heat fluxes due to its two-dimension heat spreading feature. The basic principle of operation of a vapor chamber is well understood. It uses a passive two-phase fluid to transfer heat from the evaporator to the condenser surface. The vapor chamber is a confined space with wick structure for liquid transport. The effective thermal conductivity for vapor chamber is much superior to the solid metal. There had been some studies [3,4] employing heat pipe and heat spreader for the LED cooling. Boukhanouf et al. [5] used IR camera to compare the performance between a solid copper and a copper vapor chamber. They found that the spreading resistance is reduced from 0.0278 °C W^{-1} (solid copper) to 0.0007 °C W^{-1} (vapor chamber)

* Corresponding author. Address: EE474, 1001 University Rd., National Chiao Tung University, Taiwan. Tel.: +886 3 5712121x55105; fax: +886 3 5720634.
E-mail address: ccwang@mail.nctu.edu.tw (C.-C. Wang).

http://dx.doi.org/10.1016/j.ijheatmasstransfer.2014.06.056
0017-9310/

at a supplied heat flux of 28 W cm^{-2}. Wang et al. [6] found that the effective thermal conductivity for a vapor chamber is as high as 870 $Wm^{-1}K^{-1}$ for a vapor chamber in a heat dissipation thermal module applicable for LED cooling.

Normally, the wick structure of a typical vapor chamber normally employs the sintering process. This process may imperil the integration and packaging of the LED chips. Hence an alternative solution is to employ MEMS fabrication for a micro vapor chamber based on silicon technology. The wick structure is made available through this etching process [7–9]. Through this method, integration of the LED chip and the thermal module is easier materialized, and the thermal expansion of the associated micro vapor chamber is compatible with the manufacturing process of IC industry. Accordingly, micro vapor chamber can be integrated into the LED package for effective local hot spot removal. However, currently the silicon based micro vapor chamber adopted a three layer deign [10–12] where the upper and lower layer encompass the micro channels and the middle layer contains supporting structure. The design is effective in practical application. However, since the performance of the micro vapor chamber strongly depends on the two-phase flow phenomenon within the vapor chamber. The foregoing designs can only give an overall performance of the vapor chamber and the detailed flow phenomenon within the micro vapor chamber is not clearly known. In addition to the aforementioned studies, there are some other researches that were directly linked with the heat transfer performance [13–16] of various micro flat heat pipe designs that are relevant to the present study. The associated comparison of the related references and the corresponding experimental conditions are tabulated in Table 1. As shown in the table, it appears that [15] is the only previous studies that provides visual observation of the copper based micro vapor chamber applicable to horizontal arrangement. From the application consideration, silicon based vapor chamber can be more attractive for it conglomerates nicely with the semi-conductor manufacturing process. In this regard, it is the objective of this study to examine the flow pattern alongside the micro wick structure within the micro vapor chamber for an elaborate understanding of the operation of the micro vapor chamber subject to a much wider inclination. The observation is made available through an integration of a double layer design which contains a base silicon heat spreader and an upper glass layer for flow observation.

2. Experimental setup

A schematic of the apparatus used in the experiment is shown in Fig. 1. In addition to the micro vapor chamber sample, the experimental design involved an evaporator section, a water loop, which served as a condenser, measurement devices, a data-acquisition system and an image recording system. The evaporator section was made of a copper block (35 × 7 mm), where a power supply (GW PSM-6003) supplies heat into the heater embedded in the copper block. To minimize the heat loss from the heater to the environment, a Bakelite board that has a low thermal conductivity was installed beneath the copper block. For the cooling water loop, the temperature of the water flow is maintained by a low temperature thermostat, and the cooling water was circulated in a flow rate of 10 ccm by a gear pump (Cole-Parmer, EW-75211-10). The corresponding flow rate was measured by a flow meter (Cole-Parmer, 32908-45), and a buffer and a filter were installed in the water loop to avoid particulate fouling. The description of vacuum system, fluid degassing, and filling system can be seen Tseng et al. [17] .

In this study, two micro vapor chambers having pin fin and pin fin array support structure were fabricated and tested. The working fluids tested in this study is distilled water with filling ratios being 27% and 32% for pin fin and pin fin array support structure, respectively. Detailed geometries and dimensions of the tested micro vapor chambers are shown in Fig. 2(a). The porosity for pin fin and pin fin array support layer is 0.923 and 0.954, and is 0.6 of lower layer. The micro vapor chambers were composed of silicon and glass wafers having an overall size of 35 × 40 × 1.525 mm. The micro vapor chamber contains a double layer micro structure. The lower layer is consisted of 0.15-mm-deep channels with 0.3 mm width. The micro channel is designed to provide the capillary force for liquid circulating. The depth of the upper layer is 0.45 mm with two different structures for supporting and providing space for vapor flow as shown in Fig. 2(c,d).

The test sample was fabricated using ICP-RIE after two photolithography process as depicted in Fig. 3, and a filling hole on the glass wafer was drilled using laser machining. The SEM pictures showing both kinds of wick structure, including pin fin and pin fin array support structure, in the silicon vapor chamber were shown in Fig. 4. The silicon wafer was anodically bonded to the

Table 1
Comparison of the experimental parameters of various micro flat heat pipe designs.

Investigators (year)>	Materials	Layers	Flow path geometry	Channels	Inclination angle (°)	Flow path dimensions (mm)	Working fluid	Filling ratio or volume	Q (W)	Fabrication method	Visualization
This study	Silicon	2	Rectangular channel	60	−90 to 90	0.15 × 0.3 0.2 × 0.3	Water	30%, 44%	8–20	Etching	Yes
Cai et al. [11]	Silicon	3	Pillar	–	90, −90	0.005 × 0.22 0.1 × 0.3	Ethanol, Water	0.6–3	0–10	Etching	No
Ivanova et al. [12]	Silicon	2	Pillar, rectangular channel	–	0	0.08– 0.4 × 0.1	Water	0.65 ml	0–75	Etching	No
Oshman et al. [13]	Copper, liquid crystal polymer	1	Pillar, screen	200-mesh	−90 to 90	0.2 × 0.08	Water	0.198 ml	3–12	Etching	No
Kang et al. [14]	Copper	3	Groove, screen	36, 72, 100-mesh	0	0.4 × 0.6 0.8 × 0.6 0.2 × 0.6	Methanol	0%, 41%, 57%, 82%	0–45	Etching	No
Lips et al. [15]	Copper	1	Rectangular channel	88	0	0.4 × 0.4	Methanol	[a]Filling ratio = 2.8, 1.6, 1.3	15–203	Machining	Yes
Berre et al. [16]	Silicon	2	Triangular channel	25	0	0.23 × 0.17 0.5 × 0.34	Methanol, Ethanol	0–66%	2–4	Etching	No

[a] The filling ratio V^* is defined as the total liquid volume in the flat heat pipe V_{liq} minus the dead volume due to the valve V_0, over the volume of the grooves V_{gr}: $V^* = (V_{liq} - V_0)/V_{gr}$.

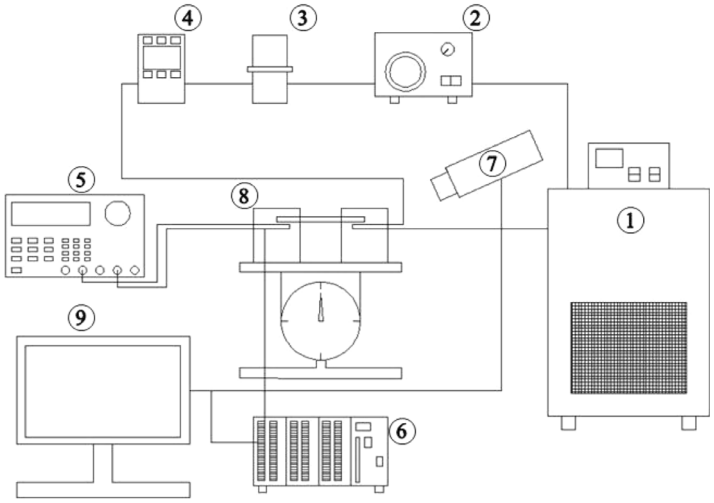

(a)

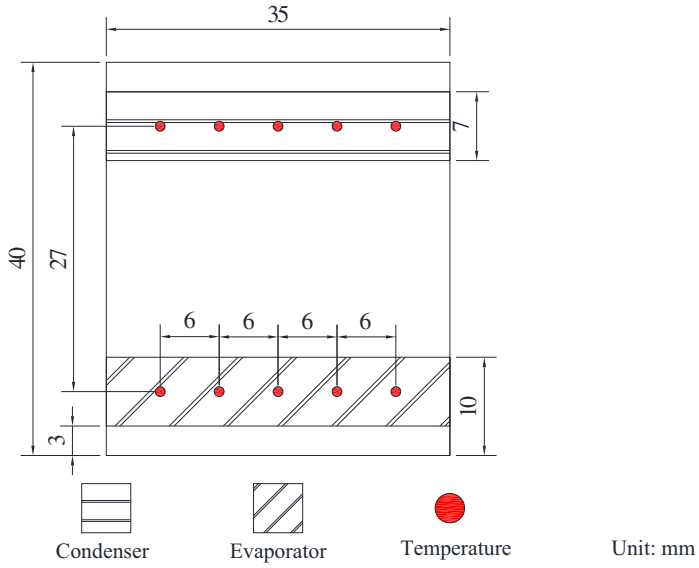

(b)

Fig. 1. (a) Test facility (b) placement of the temperature measurements.

glass wafer. After filling the micro vapor chamber with the working fluid and sealing is imposed on the fluid filling port. For further comparison, a "Silicon-Glass" sample, which had the identical dimension as the micro vapor chamber was made by anodic bonding of a silicon and glass wafer, was also tested in this study.

Thermocouples were used to measure the surface and fluid temperature. A total of 10 T-type thermocouples were placed underneath the test section to measure the average surface temperature, as schematically shown in Fig. 1(b), and two additional thermocouples were used to record the inlet and outlet temperatures of the cooling water in the condenser. These data signals were individually recorded and then averaged. During the isothermal test, the variation of these thermocouples was within 0.2 °C. In addition, all the thermocouples were pre-calibrated using a quartz thermometer that had a precision of 0.01 °C. The calibrated thermocouples had an accuracy of 0.1 °C. All the data signals were collected and converted using a data acquisition system (a hybrid recorder, Yokogawa MX-100). The data acquisition system then transmitted the converted signals through an Ethernet interface to the host computer for further operation.

Based on the measured temperature, the thermal resistance, R, is defined as follows,

$$R = \frac{T_e - T_c}{Q_a} \tag{1}$$

where T_e, T_c are the average surface temperatures in the evaporator and condenser of the heat pipe, respectively, and Q_a was estimated

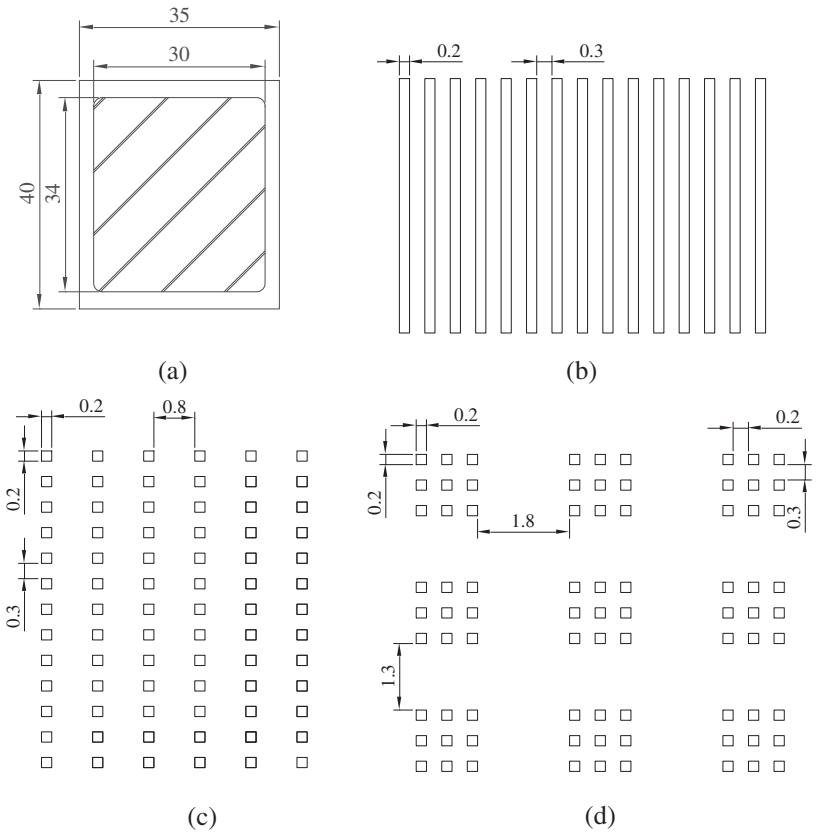

Fig. 2. Micro flat heat pipe vapor chamber (a) appearance and location of microchannel (b) microchannel at the lower layer (c) pin fin structure (d) pin fin array structure (unit: mm).

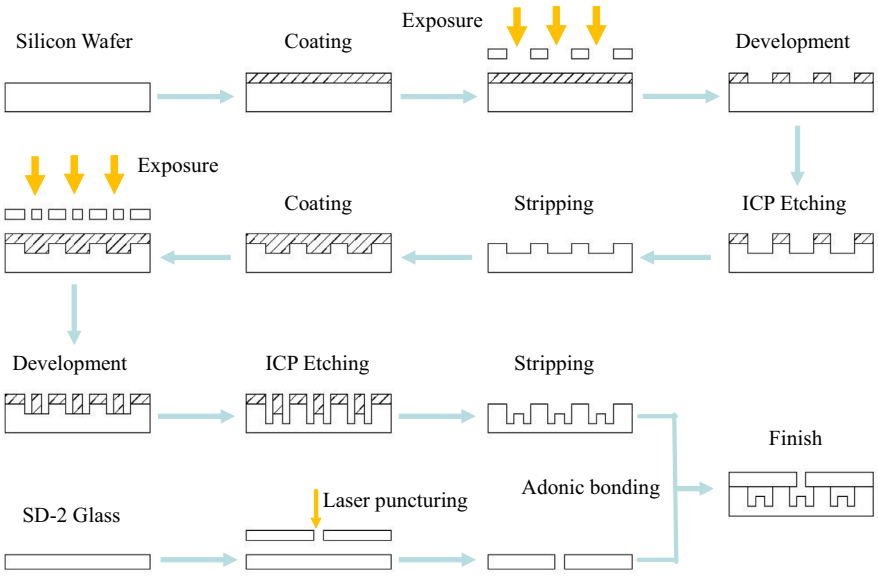

Fig. 3. Manufacturing process of the micro vapor chamber.

as the mean value of the power provided by the power supply and the heat carried away by the cooling water.

The aforementioned micro vapor chamber was located above well-fitted Bakelite. Transparent glass was fitted on the top of the test section to enable flow visualization. Observations of the flow patterns were obtained from images recorded using a high-speed video camera (Fastec HiSpec 1.2G) and a lens that could be placed at any position above the square channel.

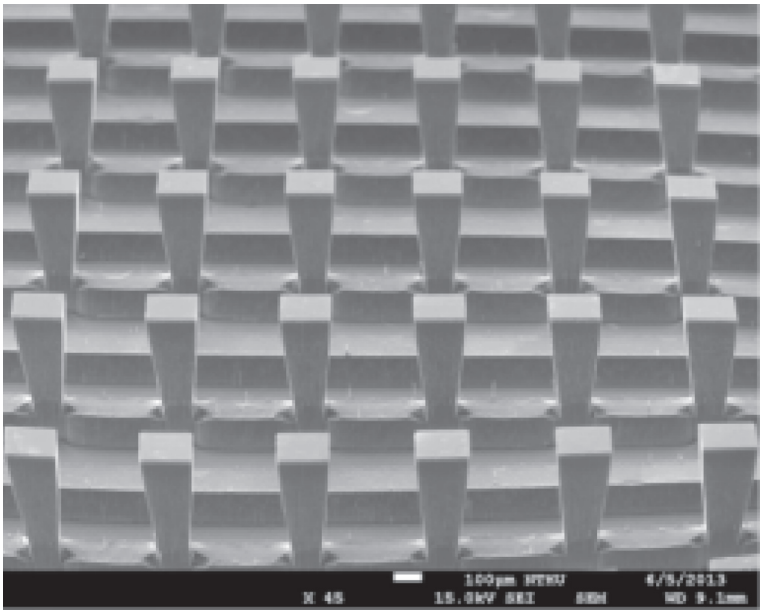

(a)

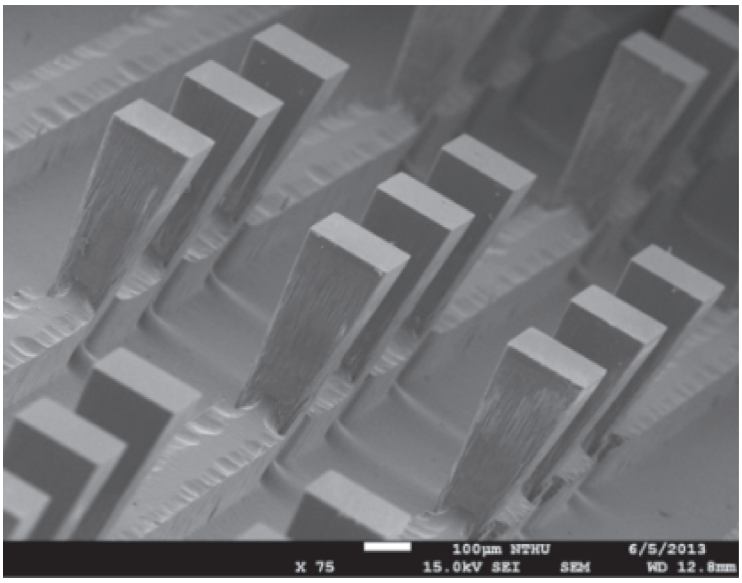

(b)

Fig. 4. SEM photos of the (a) pin fin structure (b) pin fin array structure.

3. Results and discussion

In this study, parameters affecting the performance of micro vapor chamber, including the tilt angle of the heat sources, input power, and various support of micro structure are investigated. Performance of the micro vapor chamber subject to pin fin and pin fin array structure with a vertical heat source is depicted in Fig. 5. The thermal resistance was calculated based on Eq. (1). The baseline reference is the solid silicon bonded with the glass wafer whose thermal resistance is 7.64 °C W^{-1} and it remains unchanged with the supplied power. On the other hand, the thermal resistances of the two micro vapor chambers are significantly lower than that of the solid silicon. At a supplied power of 10 W, the corresponding resistance for the pin fin and pin fin array is about 55% and 20% of the thermal resistance of the solid silicon, implying a significant improvement of the micro vapor chambers. However, the performance of these two micro vapor chambers shows opposite trend with the supplied power. For the pin fin structure, the thermal resistance is moderately increased with the rise of supplied power. Conversely, the thermal resistance pin fin array tends to be lower with the increase of the supplied power. At a supplied power of 18 W, the thermal resistance for pin fin array is only 1.32 °C W^{-1} whereas it is as high as 4.51 °C W^{-1} for the pin fin structure.

To explain the gigantic difference, one can resort to the high speed visual recording of the flow pattern as shown in Fig. 6. Normally, the thermal resistance of heat pipes is reduced when the supplied power is increased. This is mainly associated with higher vapor flow being generated, thereby leading to a higher heat transfer performance and a lower thermal resistance accordingly.

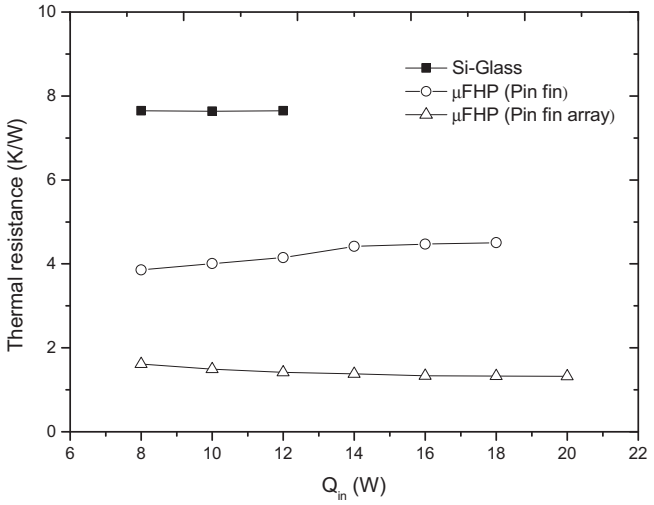

Fig. 5. Thermal resistance vs. supplied power for the tested vapor chambers and solid silicon.

It should be noted that this is often the case when the heating surface remains comparatively wet to sustain effective evaporation. However, as clearly seen in Fig. 6(a–c) applicable for the pin fin structure during the raising power process, a detectable increase of the dry-out portion prevails. This eventually gives rise to a lower heat transfer performance. In addition, from the observed window region of Fig. 6(a–c), the condensate shows some aggregations alongside the microchannel, this also jeopardizes effective liquid/vapor circulation, and deteriorates the heat transfer performance. In summary of these two effects, a moderate increase of the thermal resistance for the pin fin vapor chamber is encountered. Conversely, as shown in Fig. 6(d–f), the pin fin array structure does not reveal such phenomenon where the dry out portion at the left-lower corner is about the same irrespective of the rise of supplied power. The corresponding dry-out surface relative to the total surface for the two structures vs. supplied power is shown in Fig. 6(g). Apparently the dry-out surface portion of the pin fin array is always less than 20% throughout the test range but the dry out portion for the pin fin structure exceeds 40% and approaches 50% at a supplied power of 18 W.

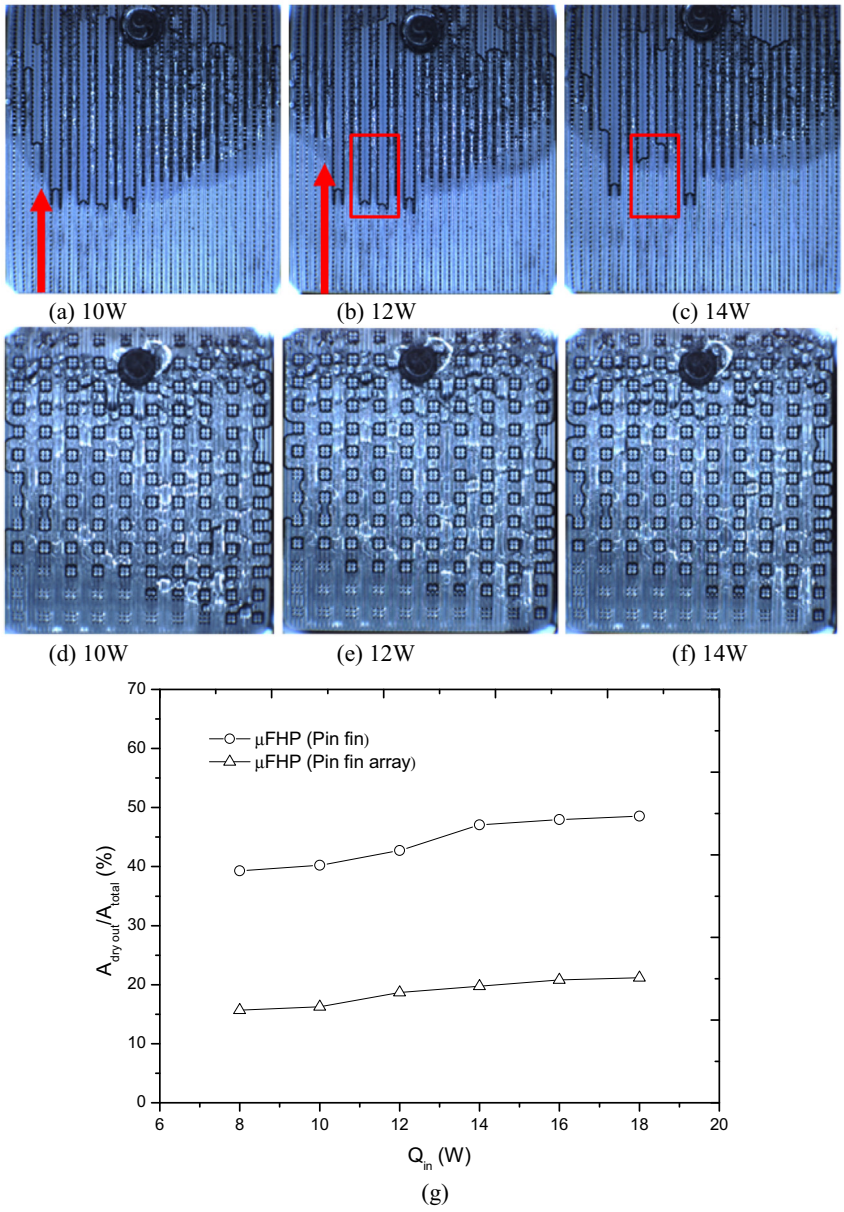

Fig. 6. Observed flow pattern for the (a–c) pin fin structure (d–f) pin fin array structure; (g) dry out ratios between pin fin structure and pin fin array structure.

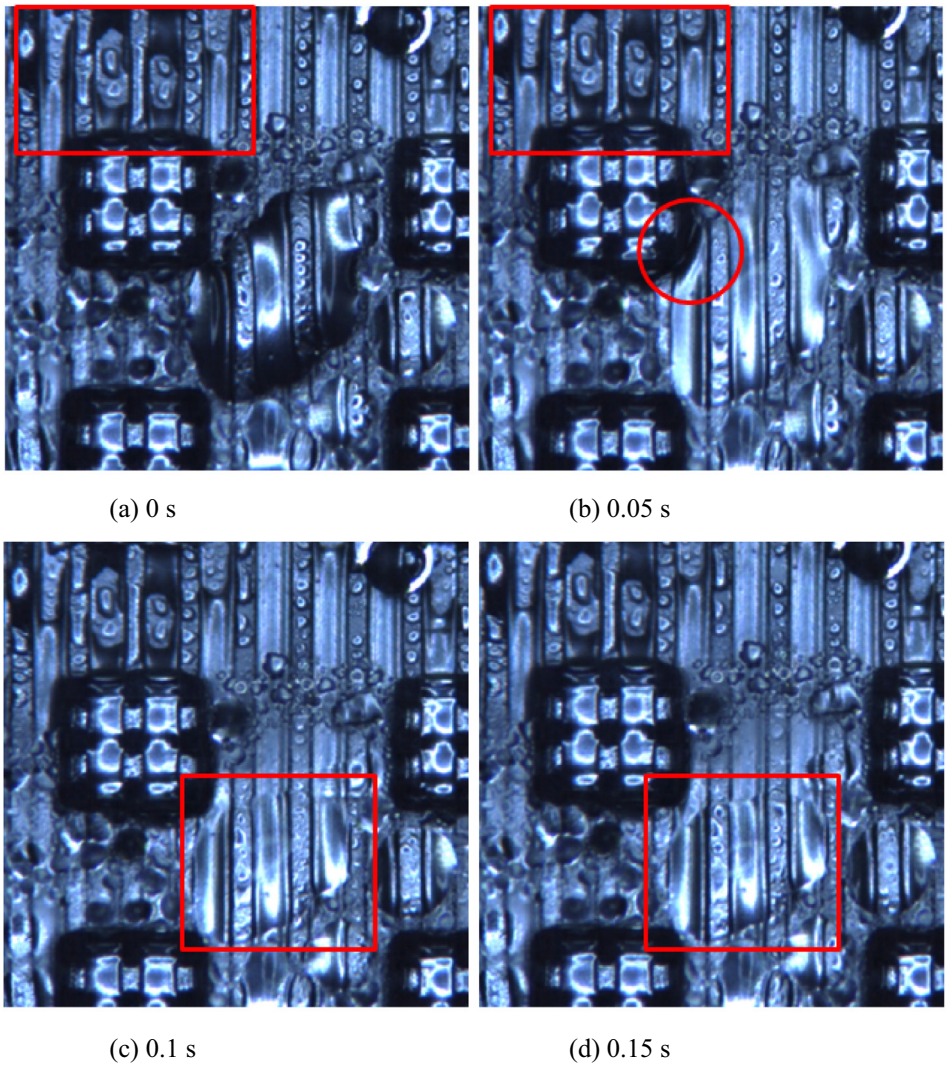

Fig. 7. Condensation flow pattern of the pin fin array vapor chamber at the upper part of the condenser.

From the observation, one can realize that there are two mechanisms counteract with each other for the micro vapor chamber when the supplied power is increased. On the positive side, a higher power brings about thinner liquid layer and develops more vapor flow which may impose a better heat transfer performance on the vapor chamber. On the down side, a higher power can also accentuate the dry out of the heating surface, yielding a lower heat transfer performance. As a result, it will result in a rise of thermal resistance if the latter mechanism offset the first one.

For a more detailed understanding of the opposite performance of the pin fin array structure, the corresponding flow patterns at the upper part and at the channel of the condenser are schematically shown in Figs. 7 and 8. The flow pattern in the condensing portion is shown in Fig. 7(a–d). From the observed window outlined in the figure, one can see the condensate droplet forms on the channel as well as the glass surface, and the droplets continue to grow as time elapses. Note that the surface is hydrophilic and the presence of pin fin structure also provide additional capillary force which results in filmwise pattern for the condensate. Once the growing droplet touches the wick structure, the liquid is soon drawing away by the capillary force to make room for condensation. Yet the related vapor flow generated from the evaporator is condensed on the microchannel. Hence, from the stable periodic heat removal, it would ensure a decrease of thermal resistance with supplied power.

In practical applications, although not often, the heat source may be placed in a certain tilt angle. The heat sources may be placed vertically, inclined or even upside down depending on the application. Hence, the effect of tilt angle on the performance of the pin fin array micro vapor chamber is examined and is shown in Fig. 9. Test results indicate that the vapor chamber is still in function even for an upside-down arrangement. The thermal resistance performance, however, is reduced with the rise of tilt angle, and the vertical arrangement gives the lowest thermal resistance. However, the thermal resistance is considerably increased if the heat source is placed upwards, and the corresponding thermal resistance for an upside-down heat source can be threefold higher than that of the vertical arrangement. The results are not surprising for the gravity is acting against the liquid condensate in the returning path. The completion of liquid/vapor circulation relies on capillary force only, yet the gravity force acts against the capillary force. In addition, one can see that the thermal resistance is moderately increased with the supplied power for tilt angles of 45° and 90°. The results can be made clear from the flow observation shown in Fig. 10 where the condensate is accumulated in the bottom of vapor chamber, thereby showing a detectable rise of dry

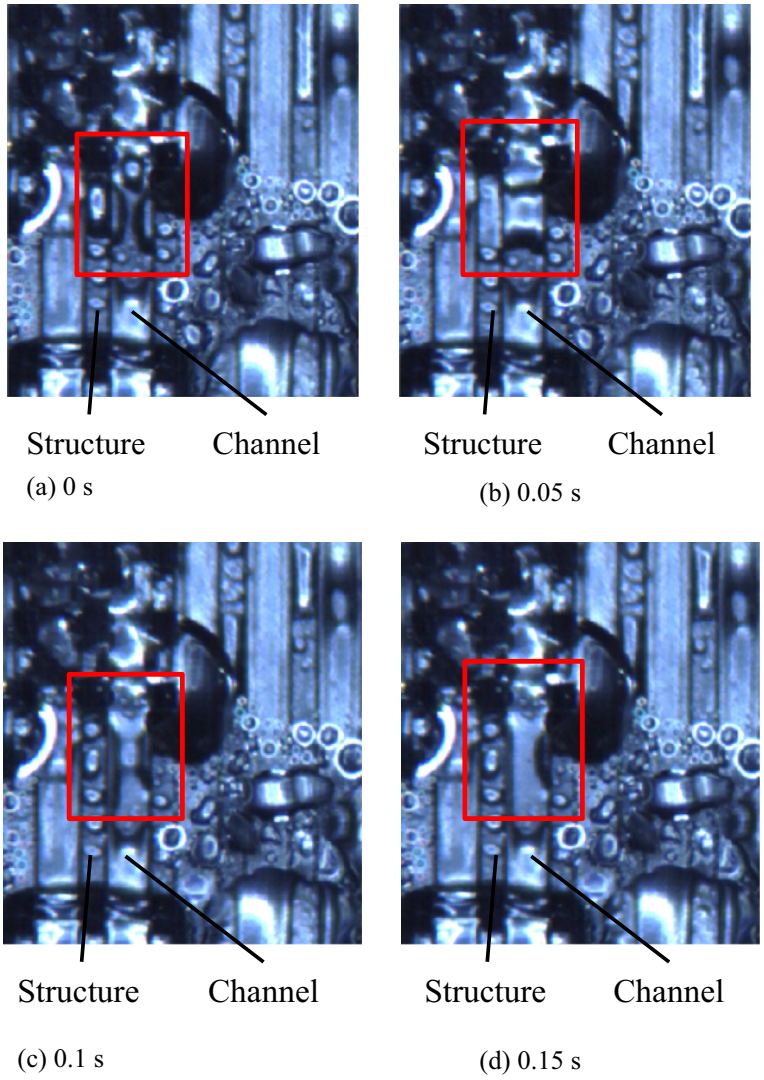

Fig. 8. Condensation flow pattern of the pin fin array vapor chamber at the channel of the condenser.

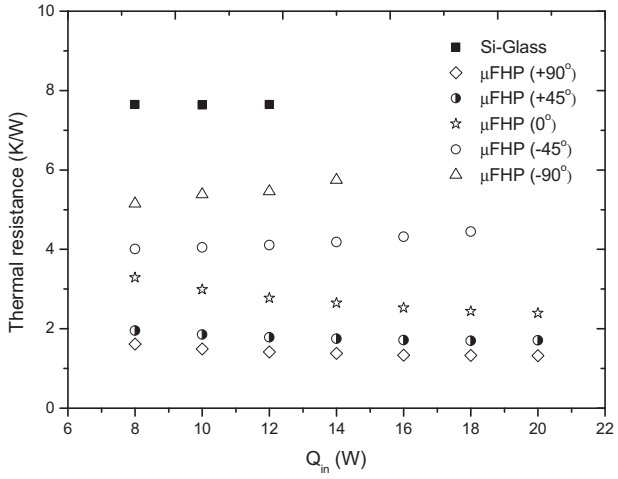

Fig. 9. Effect of tilt angle on the thermal resistance subject to various supplied power for the pin fin array vapor chamber.

out portion. As a consequence, one can see a moderate rise of thermal resistance with the increase of supplied power.

4. Conclusions

In this study, thermal performances of double layer vapor chambers are reported and their corresponding flow visualizations are conducted. Two micro vapor chambers having pin fin and pin fin array support structure were fabricated and tested. The working fluid tested in this study is distilled water with filling ratios being 27% and 32% for pin fin and pin fin array support structure, respectively. The micro vapor chambers were composed of silicon and glass wafers having an overall size of $35 \times 40 \times 1.525$ mm. The micro vapor chamber contains a double layer micro structure. The effect of the tilt angle of the heat sources, input power, and support of micro structure are investigated. Based on the foregoing discussion, the following conclusions are made:

(1) Both the pin fin and pin fin array vapor chambers show appreciably lower thermal resistance as compared to the solid silicon counterpart, the thermal resistance of the pin fin vapor chamber is about 52–60% of the solid silicon whereas the corresponding thermal resistance of the pin fin array is only 17–20% of the solid silicon.

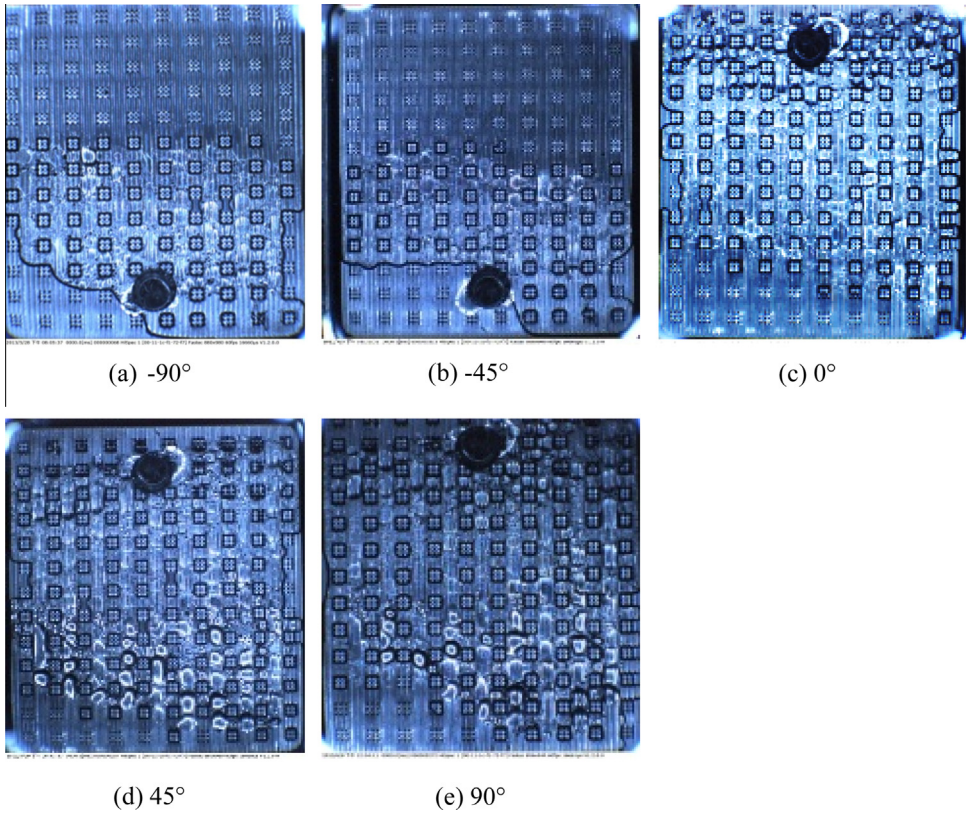

Fig. 10. Photos of the observed two phase flow pattern for the pin fin array vapor chamber subject to various tilt angles.

(2) The thermal resistance of the pin fin vapor chamber is moderately increased with the increase of supplied power whereas opposite trend is encountered for the pin fin array. The phenomenon is associated with the influence of dry-out phenomenon.
(3) For the influence of tilt angle with the pin fin array vapor chamber, it is found that the vapor chamber is still in function even for an upside-down arrangement. The thermal resistance, however, is reduced with the rise of tilt angle, and the vertical arrangement gives the lowest thermal resistance. However, the thermal resistance is considerably increased if the heat source is placed upwards, and the corresponding thermal resistance for an upside down heat source can be threefold higher than that of the vertical arrangement.

Conflict of interest

None declared.

Acknowledgments

The authors are indebted to the financial support from the Bureau of Energy of the Ministry of Economic Affairs, Taiwan and grants from National Science Council, Taiwan under contracts NSC-100-2221-E-155-066 and NSC-100-2221-E-009-087-MY3, and NSC 101-2221-E-151-024-MY3 and NSC 101-2622-E-151-016-CC3.

References

[1] http://www.digitimes.com.tw/tw/dt/n/shwnws.asp?cnlid=13&cat=20 &id=0000313143_FPK0CNTD50PRFD2G9R2H0&ct=1, in.
[2] A. Christensen, S. Graham, Thermal effects in packaging high power light emitting diode arrays, Appl. Therm. Eng. 29 (2–3) (2009) 364–371.
[3] L. Kim, J.H. Choi, S.H. Jang, M.W. Shin, Thermal analysis of LED array system with heat pipe, Thermochim. Acta 455 (1–2) (2007) 21–25.
[4] H. Zhong, C. Zhong, W. Mingguang, Heat dissipation for LED lighting: vapor chamber substrate printed circuit board, in: 2010 the 5th IEEE Conference on Industrial Electronics and Applications (ICIEA), 2010, pp. 565–570.
[5] R. Boukhanouf, A. Haddad, M.T. North, C. Buffone, Experimental investigation of a flat plate heat pipe performance using IR thermal imaging camera, Appl. Therm. Eng. 26 (17–18) (2006) 2148–2156.
[6] J.C. Wang, R.T. Wang, T.L. Chang, D.S. Hwang, Development of 30 Watt high-power LEDs vapor chamber-based plate, Int. J. Heat Mass Transfer 53 (19–20) (2010) 3990–4001.
[7] C. Gillot, Y. Avenas, N. Cezac, G. Poupon, C. Schaeffer, E. Fournier, Silicon heat pipes used as thermal spreaders, IEEE Trans. Compon. Pack. T 26 (2) (2003) 332–339.
[8] S.W. Kang, S.H. Tsai, H.C. Chen, Fabrication and test of radial grooved micro heat pipes, Appl. Therm. Eng. 22 (14) (2002) 1559–1568.
[9] S. Launay, V. Sartre, M. Lallemand, Experimental study on silicon micro-heat pipe arrays, Appl. Therm. Eng. 24 (2–3) (2004) 233–243.
[10] Q.J. Cai, A. Bhunia, C.L. Tsai, M.W. Kendig, J.F. DeNatale, Studies of material and process compatibility in developing compact silicon vapor chambers, J. Micromech. Microeng. 23 (6) (2013).
[11] Q.J. Cai, B.C. Chen, C.L. Tsai, Design, development and tests of high-performance silicon vapor chamber, J. Micromech. Microeng. 22 (3) (2012).
[12] M. Ivanova, A. Lai, C. Gillot, N. Sillon, C. Schaeffer, F. Lefevre, M. Lallemand, E. Fournier, Design, fabrication and test of silicon heat pipes with radial microcapillary grooves, in: The Tenth Intersociety Conference on Thermal and Thermomechanical Phenomena in Electronics Systems, 2006, ITHERM '06, 2006, pp. 545–551.
[13] C. Oshman, B. Shi, C. Li, R.G. Yang, Y.C. Lee, G.P. Peterson, V.M. Bright, The development of polymer-based flat heat pipes, J. Microelectromech. Syst. 20 (2) (2011) 410–417.
[14] S.W. Kang, S.H. Tsai, M.H. Ko, Metallic micro heat pipe heat spreader fabrication, Appl. Therm. Eng. 24 (2–3) (2004) 299–309.
[15] S. Lips, F. Lefevre, J. Bonjour, Nucleate boiling in a flat grooved heat pipe, Int. J. Therm. Sci. 48 (7) (2009) 1273–1278.
[16] M. Le Berre, S. Launay, V. Sartre, M. Lallemand, Fabrication and experimental investigation of silicon micro heat pipes for cooling electronics, J. Micromech. Microeng. 13 (3) (2003) 436–441.
[17] C.Y. Tseng, K.S. Yang, K.H. Chien, M.S. Jeng, C.C. Wang, Investigation of the performance of pulsating heat pipe subject to uniform/alternating tube diameters, Exp. Therm. Fluid Sci. 54 (2014) 85–92.